geomatics

MDPI

Article

TLS-Based Assessment of Building Tilt, Torsional Deformation and Structural Response to Mining-Induced Ground Movements

Robert Gradka [1,*], Andrzej Kwinta [2] and Zbigniew Muszyński [1]

[1] Department of Geodesy and Geoinformatics, Faculty of Geoengineering, Mining and Geology, Wroclaw University of Science and Technology, 50-370 Wrocław, Poland; zbigniew.muszynski@pwr.edu.pl
[2] Department of Geodesy, Faculty of Environmental Engineering and Geodesy, University of Agriculture in Krakow, 31-120 Kraków, Poland; andrzej.kwinta@urk.edu.pl
* Correspondence: robert.gradka@pwr.edu.pl

Highlights

What are the main findings?

- TLS analysis of 123 horizontal cross-sections, including 111 valid rotational estimates, revealed global building tilt, an overall increasing torsional rotation with height despite local variations, and a spatially variable structural response in an eleven-storey residential building affected by mining activity.
- Comparison with a mining-induced ground deformation model showed that the measured structural response does not directly reproduce ground movements because of structural stiffness and soil–foundation–structure interaction.

What are the implications of the main findings?

- Assessment of mining-induced building deformation should combine ground deformation models with direct geometric measurements of the structure.
- TLS provides an effective engineering tool for diagnosing complex deformation mechanisms that cannot be reliably identified using conventional surveying methods alone.

Abstract

Ground deformations induced by underground mining significantly affect the geometric condition and serviceability of buildings located in mining areas. Conventional assessments are commonly based on ground deformation indicators, which do not necessarily reflect the actual structural response. This study presents a terrestrial laser scanning (TLS)-based methodology for assessing the three-dimensional deformation of an eleven-storey residential building located in the Legnica–Głogów Copper District (LGCD), Poland. The analysis was performed using a high-density point cloud acquired from ten scanning positions. Following registration and filtering, building geometry was reconstructed and corner positions were determined from 123 horizontal cross-sections. Horizontal displacements, tilt profiles, and rotation about the vertical axis were subsequently analysed within a local coordinate system. The results revealed pronounced spatial variability in both displacement magnitude and direction. The maximum horizontal displacement reached approximately 0.18 m, corresponding to a local tilt of 5.9 mm/m. Corner displacements at the highest common observation level ranged from 8.6 mm to 178.3 mm, indicating that the observed geometry is inconsistent with a simple rigid-body model subjected to uniform tilting. Analysis of geometric changes with height further identified an overall increase in torsional rotation with height, accompanied by local variations. Comparison of TLS-derived geometry with a theoretical mining-induced ground deformation model showed that the measured structural response does not directly reproduce the underlying

Check for updates

Academic Editor: Alessandro Vitale

Received: 29 June 2026
Revised: 21 August 2026
Accepted: 26 August 2026
Published: 1 September 2026

Copyright: © 2026 by the authors. Licensee MDPI, Basel, Switzerland. This article is an open access article distributed under the terms and conditions of the Creative Commons Attribution (CC BY) license.

ground deformation pattern. The largest discrepancies occurred along the building longitudinal axis, indicating that structural stiffness and soil–foundation–structure interaction significantly modify the transfer of ground movements to the superstructure. These results demonstrate the capability of TLS for detailed assessment of mining-affected buildings and provide quantitative insight into the relationship between ground deformation and actual structural response.

Keywords: terrestrial laser scanning (TLS); mining-induced subsidence; building tilt; torsional deformation; point cloud analysis; deformation monitoring; engineering surveying; soil–structure interaction

1. Introduction

Underground mining activities conducted beneath urbanized areas represent one of the principal sources of anthropogenic ground deformation. Mining-induced ground movements may result in subsidence, ground tilt, curvature, horizontal strain, and, under specific geological and mining conditions, discontinuous deformations such as fissures, faults, and sinkholes [1–6]. Consequently, mining regions require continuous deformation monitoring, particularly where mining operations are conducted in close proximity to residential buildings and critical infrastructure [7].

In Poland, the Legnica–Głogów Copper District (LGCD) constitutes one of the most significant examples of a mining area affected by long-term underground extraction. Decades of copper ore mining have generated complex rock mass displacements and ground surface deformations. Numerous studies have confirmed both the applicability of conventional prediction methods and the necessity of their continuous verification through field measurements [8–13]. Recent research increasingly combines traditional surveying approaches with remote sensing techniques to enable continuous and multi-scale monitoring of mining subsidence basins [14]. This issue is particularly relevant in mining cities such as Polkowice, where residential buildings have been subjected to long-term mining influences for several decades [15].

High-rise and mid-rise residential buildings, especially those constructed using large-panel prefabricated technology, are particularly sensitive to mining-induced ground movements. Owing to their substantial spatial stiffness, ground deformations may induce global tilting, torsional distortion, redistribution of internal forces, damage to non-structural elements, and deterioration of serviceability conditions. The response of buildings to differential settlement has been extensively investigated in geotechnical and structural engineering research, highlighting the fundamental role of structural stiffness and soil–structure interaction [16,17]. Under mining conditions, these effects may be further intensified by spatially variable ground deformation and asymmetric mining influences.

In recent years, significant advances have been made in non-contact geometric monitoring techniques, including terrestrial laser scanning (TLS), close-range photogrammetry, and satellite-based interferometric synthetic aperture radar (InSAR). Among these methods, TLS has become a widely applied tool for structural diagnostics, geometric analysis, and deformation monitoring due to its high point density, high spatial resolution, and capability for detailed three-dimensional reconstruction of structures [18–24]. Previous studies have successfully applied TLS to the assessment of industrial chimneys, towers, and other slender engineering structures [25–29].

Despite the growing use of TLS in deformation monitoring, relatively limited attention has been devoted to the comprehensive three-dimensional assessment of residential buildings located in active mining areas, particularly with respect to the simultaneous

occurrence of global tilt, torsional deformation, and the relationship between ground deformation and the actual geometric response of the structure. Furthermore, studies directly comparing TLS-derived building geometry with theoretical models of mining-induced ground deformation remain scarce.

Unlike previous TLS investigations focused primarily on chimneys, towers, and other slender structures, the present study examines the spatial response of a multi-storey residential building subjected to long-term mining influences. Particular emphasis is placed on identifying global tilt, torsional deformation, and discrepancies between predicted ground deformation and the observed structural response.

The objective of this study is to assess the spatial deformation of an eleven-storey residential building located in Polkowice, Poland, using terrestrial laser scanning supported by conventional geodetic surveying techniques. The analysis includes the determination of horizontal corner displacements, evaluation of tilt development with height, assessment of torsional deformation, and comparison of the measured building geometry with a theoretical mining-induced ground deformation model. Particular attention is devoted to evaluating the degree of agreement between the TLS-derived structural response and the deformation field predicted from mining influence theory.

The results contribute to a better understanding of the long-term response of multi-storey buildings to underground mining activity and provide insight into the interaction between ground deformation, foundation behaviour, and structural stiffness. In particular, the study demonstrates that the geometric response of the building cannot be interpreted as a direct representation of ground deformation, highlighting the importance of incorporating structural behaviour into the assessment of mining impacts on buildings.

2. Study Area and Building Characteristics

This study was conducted on an eleven-storey residential building located in Polkowice, southwestern Poland, within the Legnica–Głogów Copper District (LGCD), one of the most active underground mining regions in Europe (Figure 1). The area has been affected by intensive copper ore extraction for several decades, resulting in long-term and cumulative ground surface deformations.

Underground copper ore extraction in the LGCD is carried out using the room-and-pillar mining system. The resulting mining-induced ground movements generate extensive subsidence basins accompanied by ground tilts and horizontal strains. These deformation components constitute kinematic loading acting on building foundations and may induce structural displacements, tilting, and three-dimensional deformation of building structures.

In addition to continuous ground deformation, the study area is also affected by mining-induced seismic activity, which is a common phenomenon in the LGCD. Such seismic activity may contribute to structural damage and geometric irregularities in buildings located within mining areas [30,31]. Consequently, the present geometric condition of the investigated structure should be regarded as the cumulative effect of both long-term continuous deformation processes and episodic dynamic loading associated with mining tremors.

The investigated building was constructed in the early 1970s using large-panel prefabricated reinforced concrete technology and comprises eleven above-ground storeys. The overall height of the structure is approximately 40 m. The building has a rectangular footprint of approximately 16 m $\times$ 22 m and consists of one structural segment without expansion joints. It was constructed using a large-panel prefabricated reinforced concrete system with transverse and longitudinal load-bearing walls connected by reinforced concrete floor slabs. The building is founded on reinforced concrete raft foundations and includes a basement level. The investigated structure has remained exposed to mining-

induced ground movements for more than four decades and, prior to the TLS survey, had been withdrawn from regular residential use owing to its deteriorated technical condition. Buildings of this type exhibit considerable spatial stiffness resulting from the load-bearing wall system composed of interconnected precast reinforced concrete panels. Under conditions of differential ground settlement, such structural systems possess limited capability to accommodate imposed deformations, which may lead to stress redistribution, stiffness changes, global tilting, and torsional deformation [16,17].



Figure 1. Location of the study area within Poland and general view of the investigated building. The red marking indicates the location of the investigated building.

No site-specific borehole or geotechnical investigation data directly beneath the investigated building were available to the authors; therefore, a site-specific soil stratification profile could not be reliably reconstructed and was not introduced into the analysis.

At the time of the survey campaign (April 2025), the building was unoccupied, indicating limited serviceability and justifying a detailed assessment of its geometric condition. Owing to its height, slenderness, and structural configuration, the building represents a suitable case study for investigating the response of multi-storey residential structures to long-term mining-induced ground deformation.

To facilitate the interpretation of displacement directions, a local coordinate system (LCS) was established and directly linked to the building geometry. The adopted system enabled decomposition of displacement vectors into components aligned with the principal structural directions of the building, providing a consistent basis for analysing deformation patterns and structural response.

Figure 2 presents the building footprint together with the locations of the eight corner points selected for deformation analysis. The origin of the local coordinate system (X = 0, Y = 0) was positioned near the geometric centre of the building footprint. The Y-axis was aligned parallel to the longitudinal façade, whereas the X-axis was aligned parallel to the gable wall. The coordinate system orientation was defined relative to geographic north. The azimuth of the positive Y-axis equals 103.4°, measured clockwise from geographic north. Consequently, the X-axis is perpendicular to the Y-axis and follows the right-handed coordinate system convention.

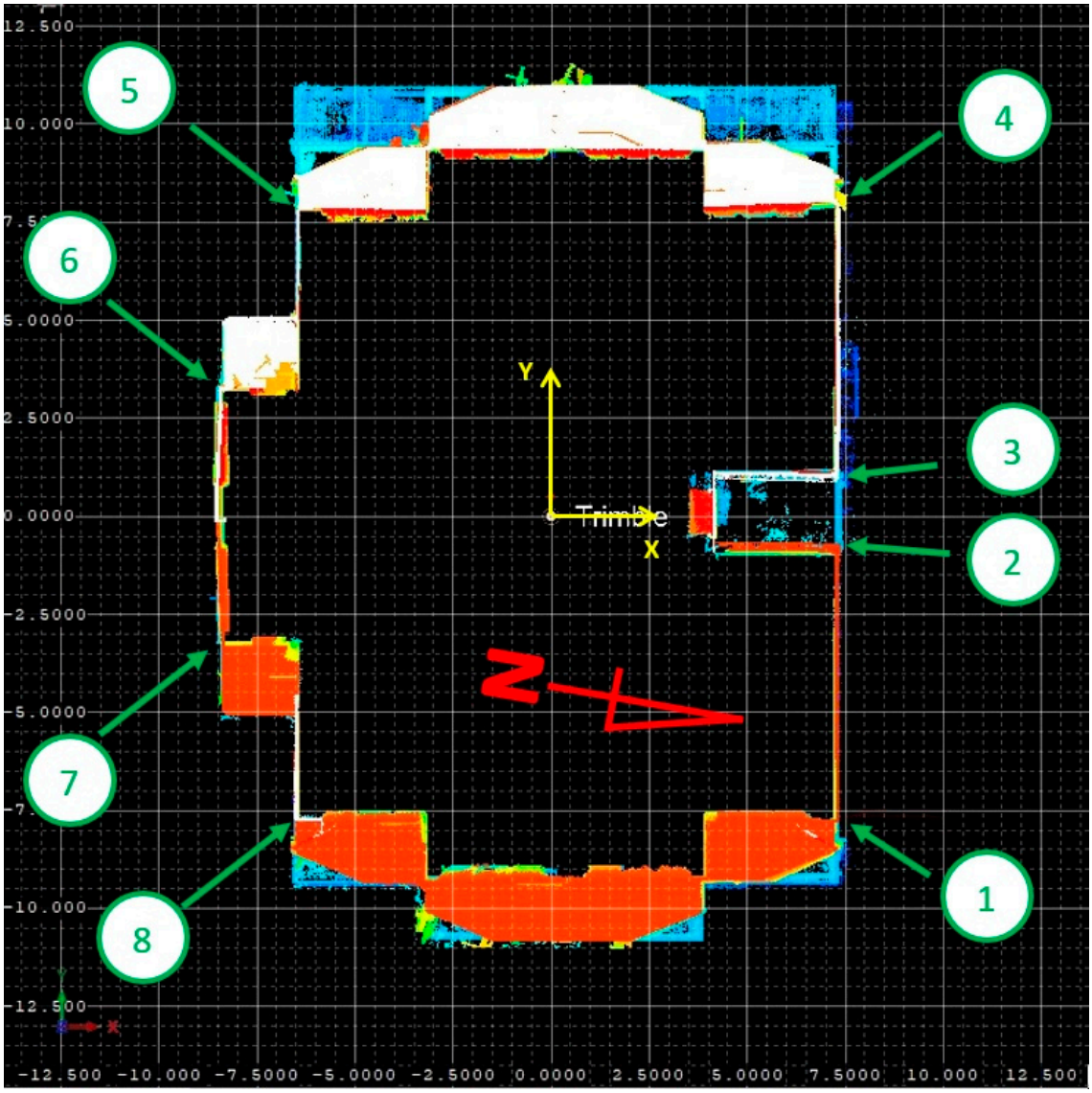


Figure 2. Ground-floor footprint of the investigated building, definition of the local coordinate system (LCS), and numbering of the analysed corner points. The green arrows and numbered markers (1–8) indicate the selected building corners used in the geometric analysis, while the yellow and red arrows indicate the local X-, Y-, and Z-axes, respectively.

The vertical reference level (H = 0) was defined at the road surface located near the pedestrian crossing in front of the main building entrance.

The adopted local coordinate system enables decomposition of displacements into longitudinal and transverse components relative to the building geometry, facilitates interpretation of tilt directions, and allows transformation of results into a global reference frame for comparison with the predicted mining-induced deformation field. The selected control points include both external and intermediate corners, enabling comprehensive reconstruction of the three-dimensional structural response, including identification of global tilt and torsional deformation mechanisms.

In TLS visualizations presented in this study, point cloud colouring is based on laser return intensity (reflectance). Higher reflectance values are represented by brighter colours, whereas lower reflectance values are represented by darker colours. White regions correspond predominantly to highly reflective surfaces, while orange and red regions indicate surfaces characterized by lower backscatter intensity.

3. Mining-Induced Ground Deformation Characteristics

The interpretation of the current geometric condition of the investigated building was supplemented by an analysis of historical ground deformation data covering the period from 1974 to 2014. This long-term dataset provides geomechanical context for the observed building deformation and allows the present geometric condition of the structure to be interpreted as the cumulative result of prolonged mining influence rather than the consequence of a single deformation event.

The historical deformation indicators presented in this section are not intended to reproduce the exact geometric condition of the building at the time of the TLS survey. Instead, they provide long-term geomechanical background describing the cumulative mining environment to which the investigated structure has been exposed over several decades. Consequently, comparisons between historical prediction data and TLS-derived building geometry should be interpreted qualitatively rather than as direct temporal validation.

It should be emphasized that the presented mining deformation data represent historical records and prediction model outputs covering the period 1974–2014. The TLS survey was performed in April 2025. Consequently, the historical deformation characteristics are used exclusively to provide long-term geomechanical context and are not intended for direct quantitative validation of the TLS-derived building geometry.

During the analysed period, cumulative ground subsidence exceeded 1.2 m. The most intensive deformation phase occurred between 1976 and 1986, corresponding to a period of intensive copper ore extraction in the study area. Subsequently, the deformation rate decreased; however, complete stabilization was not achieved, which is typical of mining and post-mining areas affected by residual and time-dependent ground movements [32–35].

Unlike short-term deformation events, mining-induced subsidence in the LGCD should be regarded as a cumulative process in which successive mining panels gradually modify the stress distribution within the rock mass and continuously alter foundation conditions. Consequently, the present geometric condition of the investigated building represents the accumulated response to many years of mining activity rather than the consequence of an individual mining operation.

From the perspective of high-rise building behaviour, ground tilt (T) represents one of the most important deformation indicators. In the investigated area, maximum tilt values reached approximately 3.0 mm/m. Ground tilt constitutes a direct kinematic load acting on building foundations and may induce global structural inclination, differential deformation, and redistribution of internal forces [16,17].

Horizontal ground strain (ε) represents another important deformation component because alternating zones of compression and extension may generate non-uniform foundation displacements. For relatively stiff reinforced concrete buildings, horizontal strain is particularly important because it may initiate differential structural response and contribute to the development of torsional deformation when the imposed ground movement is spatially non-uniform [3,4].

The deformation indicators presented in this study should therefore be interpreted as engineering descriptors of the mining environment rather than direct predictors of the observed building geometry. The actual structural response additionally depends on foundation stiffness, structural configuration, construction technology and soil–foundation–structure interaction, which modify the transfer of mining-induced ground movements to the superstructure.

Recent studies have also demonstrated the potential of data-driven approaches for long-term prediction of post-mining land deformation, particularly where deformation exhibits nonlinear temporal behaviour and conventional model parameters or detailed geotechnical information are limited [36].

Figure 3 presents the location of the investigated building within the area affected by underground mining. The grey polygon indicates the extent of mining influence, whereas the building location and reference points used in the analysis are marked in red. The computational grid covers the immediate surroundings of the building and forms the basis for interpolation and spatial analysis of ground deformation indicators, including subsidence (S), ground tilt (T), and horizontal strain (ε).

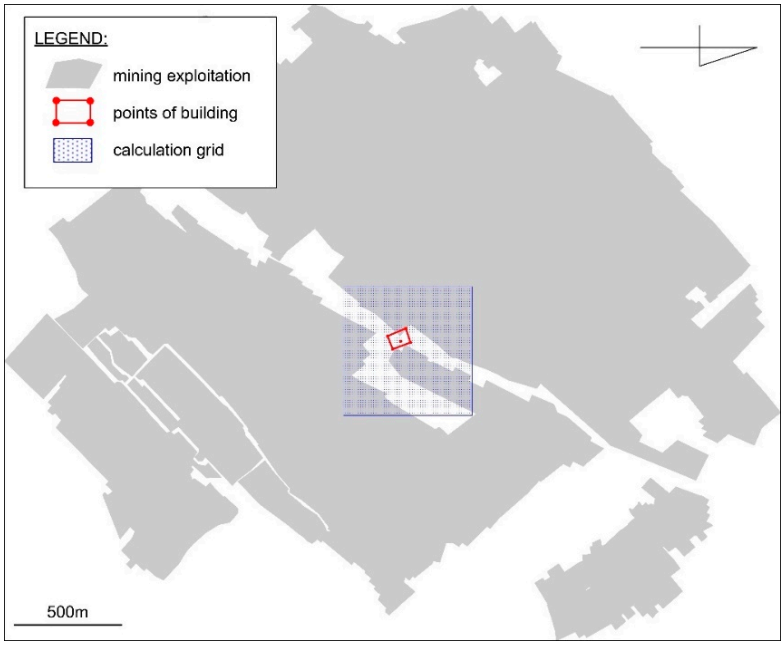


Figure 3. Location of the investigated building within the mining area and computational grid used for deformation modelling. The red outline and markers indicate the location and selected points of the investigated building.

The position of the building within the central part of the subsidence basin indicates long-term exposure to spatially variable and complex ground deformation conditions.

Figure 4 illustrates the temporal evolution of subsidence, ground tilt, and extreme horizontal strain. The subsidence curve exhibits a non-linear character, with the highest deformation rate occurring during the initial phase of mining activity. After 1990, the deformation process gradually decelerated; however, no complete stabilization was observed. The presented curves were derived from annual values obtained from the Knothe-based prediction model and subsequently smoothed for graphical presentation.

Maximum ground tilt values reached approximately 3.0 mm/m. For comparison, the maximum unit tilt derived from TLS measurements of the building geometry reached approximately 5.9 mm/m. This discrepancy suggests that the current geometric condition of the structure results from both long-term mining-induced ground deformation and the structural response of the building itself.

Temporal variations in horizontal strain reflect the development of mining activity in space and time. Alternating phases of ground compression and extension may have contributed to the formation of complex three-dimensional deformation patterns within the structure.

Figure 5 presents contour maps of subsidence, ground tilt, and horizontal strain in the vicinity of the investigated building. The deformation indicators used in this study were obtained from an available historical mining-deformation model based on Knothe's influence function theory, which is widely applied for forecasting mining-induced ground deformation in the Legnica–Głogów Copper District [1,9,13,37–39]. The present study

used these model-derived deformation indicators as a geomechanical reference field and did not independently recalibrate the model parameters from raw exploitation records. The deformation field was computed within a regular grid covering both the building footprint and its immediate surroundings. Ground tilt values were subsequently derived from spatial gradients of vertical displacement, whereas horizontal strains were calculated according to the assumptions of the adopted theoretical model. The resulting contour maps enabled assessment of the spatial variability in deformation indicators relative to the building footprint.

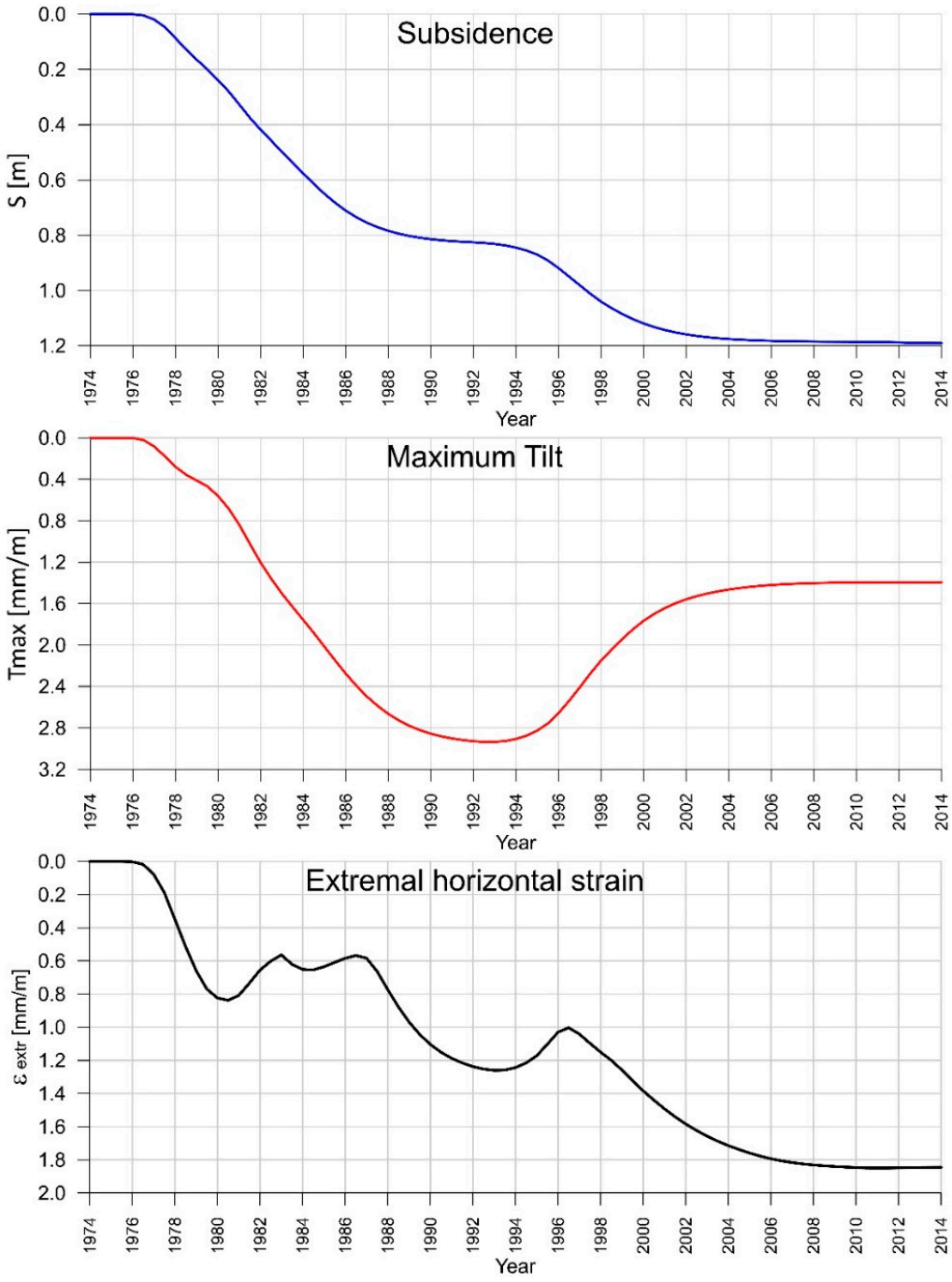


Figure 4. Historical evolution of cumulative subsidence (S), maximum ground tilt (T) and extreme horizontal strain (ε) derived from annual mining deformation predictions for the period 1974–2014. Continuous curves represent annual model outputs smoothed for graphical presentation and used exclusively for long-term geomechanical interpretation.

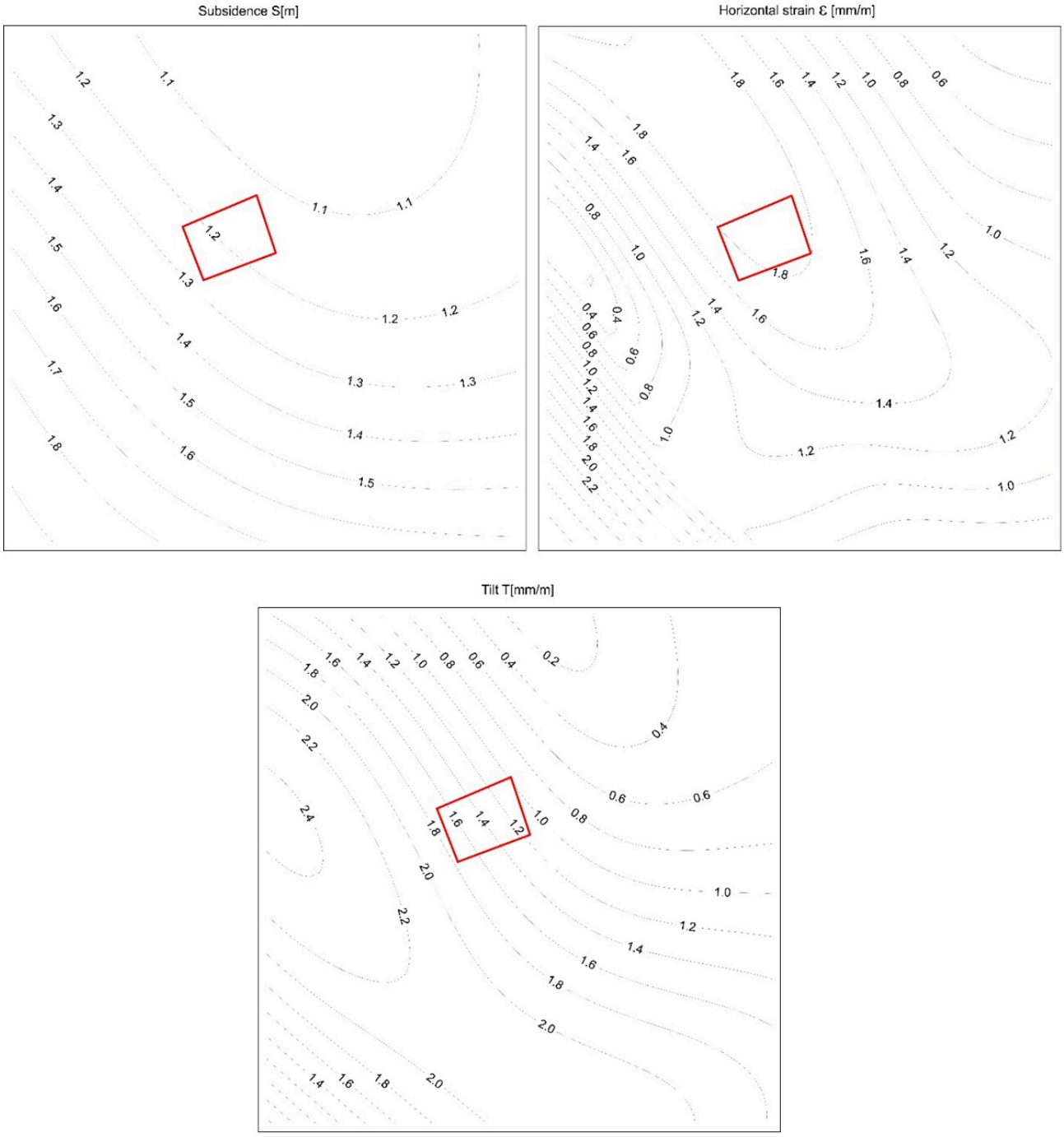


Figure 5. Spatial distribution of ground deformation indicators in the vicinity of the investigated building: subsidence (S), horizontal strain (ε), and ground tilt (T). The red marking indicates the location of the investigated building.

The identified tilt gradients and variations in horizontal strain provided the basis for interpreting the measured structural response and identifying potential deformation mechanisms. The building is located within a subsidence zone characterized by cumulative settlements of approximately 1.2–1.3 m. The horizontal strain field exhibits significant spatial gradients across the building footprint, whereas the tilt field displays a pronounced directional pattern and intersects the structure asymmetrically, reaching local values of approximately 1.6–2.0 mm/m at the end of the analysed modelling period.

These results indicate that the investigated building has been subjected to a long-term, spatially heterogeneous deformation environment. This geomechanical context

is essential for interpreting the actual geometric response of the structure derived from TLS observations and for assessing the relationship between ground deformation and structural behaviour.

4. Surveying Methodology and Data Processing

To determine the three-dimensional geometry of the investigated building, a hybrid surveying approach combining total station measurements and terrestrial laser scanning (TLS) was employed. Conventional geodetic observations were used to establish a local reference framework and determine control point coordinates, whereas TLS served as the primary source of high-density geometric data [18,20].

4.1. Geodetic Control Network and Spatial Referencing

A local geodetic control network consisting of four permanently stabilized points (A–D) was established in the vicinity of the building. The control points were positioned to provide favourable observation geometry and reliable spatial referencing of all scanner stations.

The network observations were carried out using an electronic total station. Measurements were performed in two observation sets and in both telescope positions. Network adjustment was conducted using the least-squares method [40]. The resulting mean planimetric position error was 0.37 mm, while the maximum height error did not exceed 0.9 mm.

A set of reference targets was installed on the building façades and surveyed from the control network. These targets were subsequently used for the registration and georeferencing of TLS point clouds. The LCS was therefore directly linked to the geodetic control network through the surveyed reference targets, while the deformation components derived from the Knothe-based model were transformed into the same reference frame for comparison with the TLS-derived building geometry.

4.2. Terrestrial Laser Scanning Data Acquisition

The TLS survey was conducted during a field campaign performed in April 2025 using a RIEGL VZ-400i laser scanner (made in Horn, Austria) operating at a pulse repetition rate of 1200 kHz. Data acquisition was carried out in Panorama_20 mode, corresponding to an angular resolution of 20 mdeg (0.02°) and a full 360° field of view at each scan position.

A total of ten scan stations were established around the building at distances ranging from approximately 15 m to 30 m. This configuration ensured complete geometric coverage of the structure while minimizing occlusions associated with balconies, façade recesses, and building edges [41].

In addition to laser measurements, digital images were acquired for RGB colourization of the point cloud. Data from the integrated IMU/GNSS system were used for preliminary scan orientation. The reference targets enabled target-based registration and accurate transformation of all scans into the local geodetic reference frame.

4.3. Point Cloud Registration and Filtering

Point cloud processing was performed in the RiSCAN PRO (ver. 2.9) software environment. Initially, individual scans were roughly oriented using IMU/GNSS observations. Subsequently, a rigorous multi-station adjustment procedure was performed using both target-based registration and cloud-to-cloud matching techniques.

The registration residuals were within the range of approximately 3–5 mm.

The registered point cloud was then subjected to a filtering procedure comprising:

- Removal of isolated points and measurement noise;

- Elimination of objects not belonging to the building structure (vegetation, vehicles, and other temporary objects);
- Removal of secondary reflections and artefacts associated with glass surfaces;
- Selection of high-quality points based on reflectance and deviation parameters.

No separate statistical threshold was applied to classify individual points as measurement noise or artefacts; the filtering was based on geometric isolation, object classification, reflection behaviour, and the quality parameters available in the RiSCAN PRO processing workflow.

The adopted quality-control procedure reduced the influence of instrumental and environmental errors and follows current best practices in TLS-based structural deformation monitoring [21,24].

The final output consisted of a filtered point cloud representing the actual geometry of the building (Figure 6).

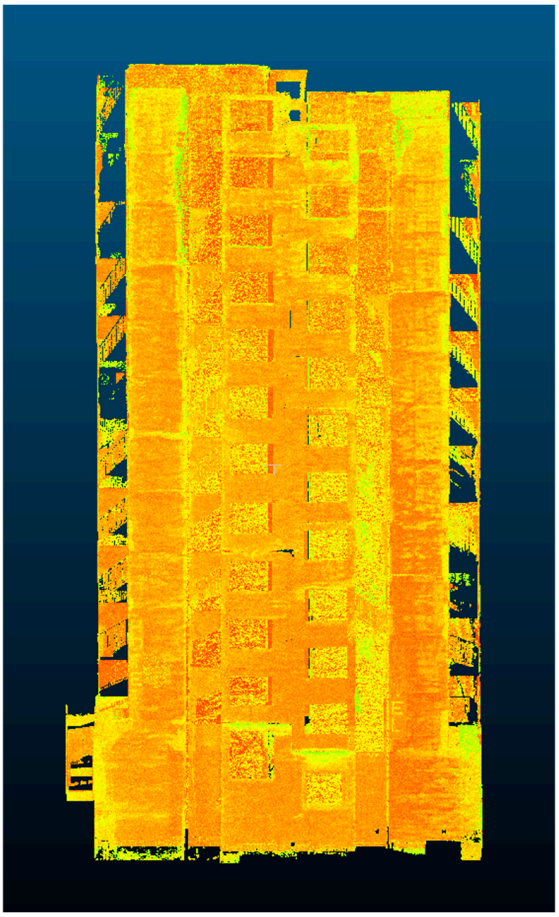


Figure 6. Registered and filtered point cloud representing the investigated building (eastern façade view).

The figure presents the final three-dimensional model obtained after registration and filtering. The resulting point cloud served as the basis for all subsequent geometric analyses, including the identification of wall planes, structural edges, and building corners.

4.4. Local Coordinate System and Cross-Section Generation

The registered point cloud was transformed into the previously defined local coordinate system (LCS) associated with the building geometry. To analyse structural deformation, horizontal cross-sections were generated at 123 elevation levels.

The cross-sections were generated at regular vertical intervals of approximately 0.25 m throughout the height of the building. This approach provided a dense sampling of the structure and enabled detailed identification of displacement gradients, local geometric irregularities, and deformation patterns as a function of elevation.

4.5. Corner Extraction and Tilt Determination

For each horizontal cross-section, the façade segments forming individual building corners were identified and modelled using a least-squares fitting procedure. The intersections of adjacent wall planes were subsequently determined and treated as representative corner positions. The positional accuracy of each corner depends not only on the precision of the fitted façade lines but also on the angle between adjacent wall segments and the effective length of the fitted line segments. For nearly orthogonal intersections, the propagated uncertainty remains close to the uncertainty of the fitted lines, whereas acute intersection angles amplify the coordinate uncertainty of the intersection point.

To ensure geometric consistency, façade segments were extracted only from continuous load-bearing wall surfaces. Balcony slabs, window recesses, façade offsets and architectural details were excluded from the least-squares fitting procedure. Consequently, identical structural wall lines were analysed throughout the entire building height.

This approach is consistent with contemporary methods for building geometry reconstruction from point cloud data [42,43].

For each corner and elevation level, the coordinates (X, Y, H) were determined within the local coordinate system (LCS).

Horizontal displacements were defined as the differences between corner coordinates at a given elevation level and the corresponding coordinates at the reference level located at the building base:

$$\begin{aligned} dX &= X_H - X_0 \\ dY &= Y_H - Y_0 \end{aligned} \quad (1)$$

where

dX—horizontal displacement component along the local X-axis [m];

dY—horizontal displacement component along the local Y-axis [m];

X_H, Y_H—coordinates of a corner at elevation H [m];

X_0, Y_0—coordinates of the same corner at the reference level [m].

Based on the displacement components, the resultant horizontal displacement magnitude was calculated as (2):

$$W = \sqrt{dX^2 + dY^2} \quad (2)$$

where

W—resultant horizontal displacement (tilt vector magnitude) [m].

The calculated parameters describe the actual horizontal displacement of each building corner relative to the reference level and provide the basis for the subsequent analysis of tilt development, deformation profiles, and spatial structural response.

The direction of displacement was characterized by the azimuth of the displacement vector determined in the local coordinate system, enabling interpretation of the dominant deformation direction relative to the building geometry.

4.6. Removal of the Translational Component

To separate rigid-body translation from the internal deformation of the structure, additional parameters were computed with respect to the geometric centre (centroid) of

each horizontal cross-section. The centroid coordinates at elevation level H were determined as the arithmetic mean of the coordinates of all identified building corners:

$$\begin{aligned} X_C^H &= \frac{1}{n}\sum_{i=1}^{n} X_i^H \\ Y_C^H &= \frac{1}{n}\sum_{i=1}^{n} Y_i^H \end{aligned} \tag{3}$$

where

X_C^H, Y_C^H—centroid coordinates at elevation H [m];
X_i^H, Y_i^H—coordinates of the i-th corner at elevation H [m];
n—number of corners included in the analysis (n = 8).

The horizontal translation vector of a given cross-section relative to the reference level was then determined as (4):

$$\begin{aligned} T_X^H &= X_C^H - X_C^0; \\ T_Y^H &= Y_C^H - Y_C^0 \end{aligned} \tag{4}$$

where

T_X^H—translational component of the centroid along the local X-axis [m];
T_Y^H—translational component of the centroid along the local Y-axis [m];
X_C^0, Y_C^0—centroid coordinates at the reference level [m].

The displacement components (1) corrected for the translational motion of the entire cross-section (4) were subsequently calculated as:

$$\begin{aligned} dX_i' &= \left(X_i^H - X_i^0\right) - T_X^H \\ dY_i' &= \left(Y_i^H - Y_i^0\right) - T_Y^H \end{aligned} \tag{5}$$

where

dX_i'—translation-corrected displacement of the i-th corner along the local X-axis [m];
dY_i'—translation-corrected displacement of the i-th corner along the local Y-axis [m].

These parameters describe the internal deformation of the structure independently of rigid-body translation and were used as supplementary indicators in the interpretation of deformation mechanisms, particularly for the assessment of torsional behaviour.

It should be emphasized, however, that for buildings located in mining-affected areas, the total displacement of the structure relative to the ground surface is of primary engineering significance. Therefore, the principal interpretation presented in this study is based on the absolute displacement components dX, dY which include both structural deformation and global translation induced by mining-related ground movements.

The adopted procedure enables separation of three independent deformation components:

(i) Rigid-body translation represented by centroid displacement;
(ii) Global rocking (overall building inclination);
(iii) Internal differential deformation manifested as torsional distortion after removal of the translational component.

In this framework, global rocking refers to the overall inclination of the building relative to the reference level, whereas torsional deformation refers to differential rotation of successive horizontal cross-sections about the vertical axis after removal of their translational component. Thus, the two components are distinguished geometrically rather than mechanically: rocking is evaluated from the change in the position and inclination of the building as a whole, while torsional behaviour is evaluated from the residual rotation of individual cross-sections.

4.7. Accuracy and Reliability Assessment

The adopted measurement and processing methodology provided a high level of reliability for the obtained results. The local control network established by total station observations achieved a mean horizontal positional accuracy of m_p = 0.37 mm and a maximum vertical accuracy of m_h = 0.9 mm. The accuracy of point cloud registration was estimated at 3–5 mm based on the residuals obtained during the multi-station adjustment process.

Errors associated with coordinate transformation, point cloud registration, and geometric approximation remained at the sub-centimetre level and were therefore significantly smaller than the observed structural displacements, which reached centimetre- and decimetre-scale magnitudes. Consequently, the detected deformation patterns can be considered representative of the actual geometric condition of the investigated structure rather than artefacts resulting from measurement uncertainty.

Considering the maximum observed displacement of approximately 180 mm and the upper estimate of the registration residuals of approximately 5 mm, the uncertainty corresponds to about 2.8% of the maximum displacement magnitude. The resulting signal-to-noise ratio is approximately 36, indicating that the principal deformation signal substantially exceeds the estimated measurement uncertainty.

The obtained accuracy levels are sufficient for reliable identification of both global tilting and local geometric irregularities, including torsional deformation and differential displacement of structural elements.

The applied methodology is consistent with current trends in deformation monitoring, which emphasize the integration of complementary surveying techniques and the combination of datasets characterized by high geometric accuracy and spatial completeness [19,22].

5. Results

The assessment of the building's spatial response was based on the analysis of corner displacements as a function of height, derived from TLS data in the local coordinate system. In total, 123 horizontal cross-sections (levels) were analysed.

5.1. Numerical Analysis of Building Displacements

The obtained results reveal pronounced spatial variability in deformation, with displacement magnitudes ranging from 8.6 mm to 178.3 mm. Such a wide range is inconsistent with a simple rigid-body model subjected to uniform tilting and indicates a complex three-dimensional geometric response.

The largest displacement magnitudes were observed at Corner 4 (178.3 mm), Corner 6 (111.6 mm), and Corner 7 (88.4 mm), indicating a strongly asymmetric deformation field. In contrast, the smallest displacements were recorded at Corner 1 (8.6 mm) and Corner 3 (16.1 mm). This distribution suggests both spatial variability in the underlying ground deformation and a non-uniform structural response. The large difference between Corner 4 and Corner 1 reflects their different positions within the spatially heterogeneous deformation field and the resulting differential response of the building. The resulting horizontal displacements and azimuths of the eight analysed building corners are summarized in Table 1.

Table 1. The final horizontal displacements of the eight analysed building corners determined at the highest common measurement level (Level 122).

Corner	*dX* [mm]	*dY* [mm]	W [mm]	Azimuth [deg]
1	2.8	−8.1	8.6	−70.9
2	26.4	20.3	33.3	37.6
3	5.6	15.1	16.1	69.7

Table 1. *Cont.*

Corner	*dX* [mm]	*dY* [mm]	W [mm]	Azimuth [deg]
4	13.1	177.8	178.3	85.8
5	31.6	35.3	47.4	48.2
6	95.5	−57.8	111.6	−31.2
7	50.6	−72.5	88.4	−55.1
8	−10.6	−47.7	48.9	−102.5

Particular attention was given to Corner 4, where the maximum displacement was observed. To illustrate the vertical deformation profile, detailed displacement data for this corner are presented in Table 2.

Table 2 shows the displacement profile of Corner 4 as a function of elevation. The results indicate an overall increase in displacement magnitude with height, although local variations are present. The deformation is clearly dominated by the local Y-direction component, resulting in a pronounced anisotropy of horizontal displacement.

Table 2. Horizontal displacement profile of Corner 4 in the local coordinate system *dX*, *dY* at selected elevation levels.

Level No.	X [m]	Y [m]	Elevation H [m]	*dX* [m]	*dY* [m]	Relative Height [m]
124	7.277	8.056	37.080	0.015	0.181	30.531
122	7.2925	8.064	36.580	0.013	0.178	30.031
120	7.278	8.055	36.288	0.015	0.177	29.740
110	7.276	8.043	33.789	0.014	0.165	27.240
100	7.302	8.014	31.290	0.039	0.136	24.741
90	7.288	8.023	28.790	0.025	0.146	22.241
80	7.278	7.991	26.292	0.016	0.113	19.744
70	7.274	7.989	23.793	0.011	0.111	17.244
60	7.261	7.980	21.293	−0.001	0.102	14.745
50	7.285	7.958	18.795	0.023	0.080	12.246
40	7.279	7.962	16.295	0.016	0.084	9.747
30	7.277	7.941	13.796	0.015	0.063	7.248
20	7.261	7.935	11.297	−0.001	0.057	4.748
10	7.268	7.903	8.798	0.005	0.025	2.249
1	7.263	7.878	6.549	0.000	0.000	0.000
		MIN=	−0.001			
		MAX=	0.181			

The maximum displacement of 0.181 m was recorded at the highest measurement level available for Corner 4 (Level 124), whereas the value of 178.3 mm reported in Table 1 corresponds to the highest common level (Level 122) available for all analysed corners.

At the top of the building, displacement components reached dY = 0.181 m and dX = 0.015 m, corresponding to a local tilt ratio of approximately 5.9 mm/m.

The displacement profile is non-linear, with several zones exhibiting increased displacement gradients, particularly within the middle part of the structure. This behaviour

may indicate local variations in structural stiffness, redistribution of internal forces, and a height-dependent structural response.

Differences in displacement evolution among individual corners further demonstrate that the building does not behave as an ideal rigid body. Variations in curvature and displacement magnitude indicate an asymmetric deformation pattern and a complex spatial response of the structural system.

The maximum displacement at the highest common measurement level reached 178 mm, whereas the minimum value was approximately 9 mm. Within the detailed profile of Corner 4, the maximum displacement attained approximately 181 mm.

To further investigate the deformation mechanism, displacement components corrected for global translation dX', dY' together with the corresponding rotation angle θz are presented for selected elevation levels in Table 3.

Table 3 includes representative elevations selected from the complete dataset comprising 123 cross-sections. Comparison between absolute and translation-corrected displacements indicates that global translation constitutes a significant component of the total building displacement. However, its removal does not alter the overall interpretation of the deformation mechanism.

Table 3. Translation-corrected displacement components dX' and dY' for Corner 4 and corresponding building rotation angle θz at representative elevation levels.

H [m]	dX' [m]	dY' [m]	θ_z [mrad]
37.00	−0.002	0.120	5.576
36.25	−0.006	0.116	5.651
33.75	−0.015	0.149	5.769
31.25	0.007	0.116	4.615
28.75	−0.005	0.123	4.345
26.25	−0.018	0.100	2.622
23.75	0.001	0.108	1.496
21.25	−0.013	0.090	1.151
18.75	0.002	0.059	0.527
16.25	−0.000	0.061	0.143
13.75	0.008	0.047	0.703
11.25	−0.009	0.037	0.174
9.75	−0.004	0.012	−0.279
8.00 (reference level)	0.000	0.000	0.000

5.2. Vertical Deformation Profile

Comparison of both displacement sets indicates that a substantial portion of the observed movement results from global translation of the entire structure. The corrected displacement profiles reveal the actual structural response after removing this translational component.

The obtained profiles indicate the non-linear nature of deformation and the presence of variable displacement gradients with increasing height. This behaviour indicates that the building does not act as an ideal rigid body but exhibits a complex response governed by soil–structure interaction. The corresponding displacement profiles are shown in Figure 7.

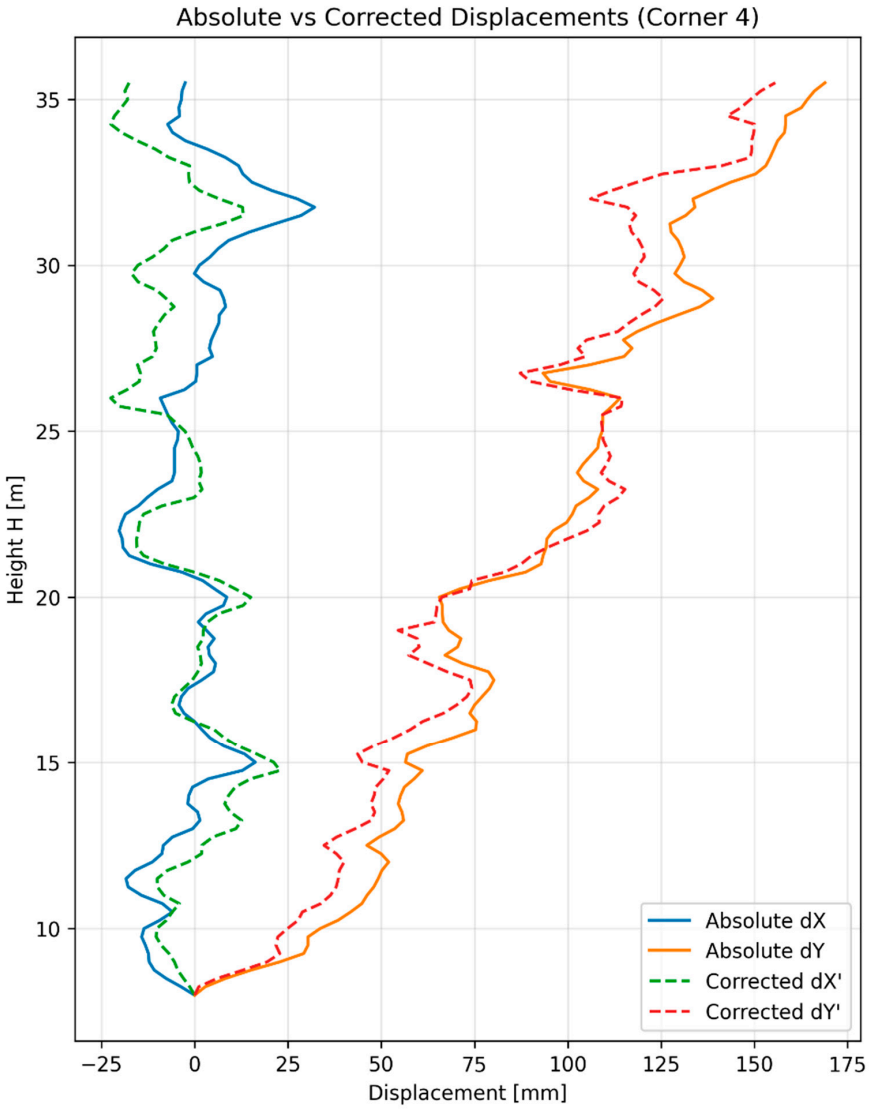


Figure 7. Vertical profiles of absolute displacement components dX, dY and translation-corrected displacements $dX^{'}$, $dY^{'}$ for Corner 4.

5.3. Vector Analysis of Corner Displacements

The vector lengths represent displacement magnitudes, whereas their orientations indicate displacement directions. The vectors are neither parallel nor uniformly distributed and exhibit substantial variability in both magnitude and orientation. This pattern demonstrates the three-dimensional character of the observed deformation. The displacement field is consistent with the coexistence of global tilting and a torsional component of the building response. The resulting horizontal displacement vectors of all analysed building corners are shown in Figure 8.

5.4. Quantitative Assessment of Building Rotation

To complement the analysis of spatial deformation, an assessment of the building rotation about the vertical axis (Z-axis) was performed. The analysis was carried out after removing the global horizontal translation component, allowing the actual structural response to be separated from rigid-body displacement of the entire structure.

The rotation angle θz was determined at successive elevation levels using a two-dimensional rigid-body transformation model. Although 123 horizontal cross-sections were generated for the building geometry analysis, 111 levels provided valid θz estimates

and were therefore included in the statistical trend analysis. The remaining levels were excluded because a reliable rotational solution could not be obtained from the available geometric configuration.

For each level, the centroid of the building cross-section was calculated and its translation relative to the reference level was removed. The rotation angle was then estimated by a least-squares adjustment minimizing the discrepancies between the initial and transformed point configurations [44].

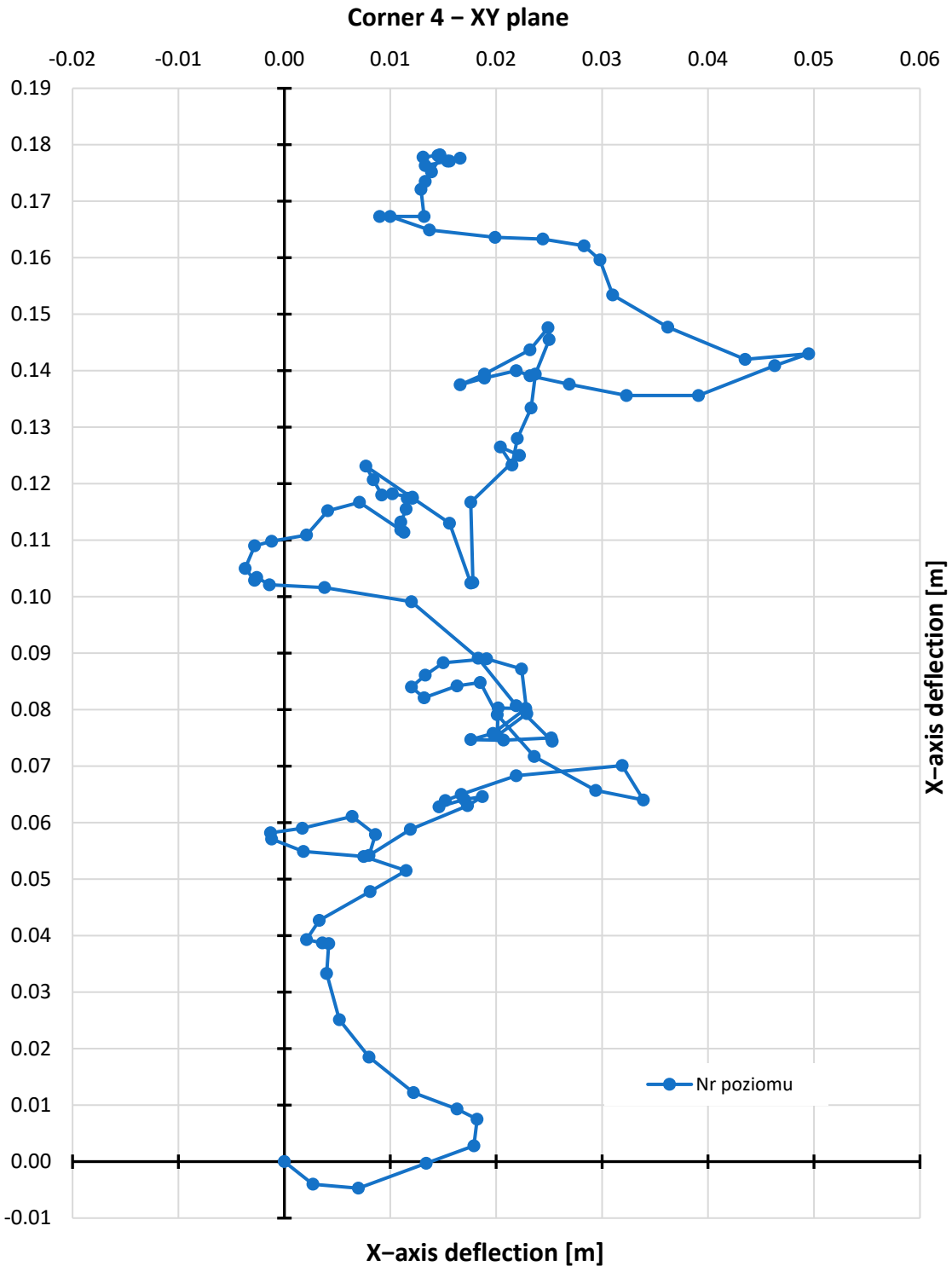


Figure 8. The horizontal displacement vectors of all analysed building corners projected onto the local XY plane.

The resulting rotation angle represents the residual geometric rotation of each horizontal cross-section after removal of its translational component and is therefore interpreted in this study as a geometric indicator of torsional deformation. The resulting elevation-dependent rotation profile is shown in Figure 9.

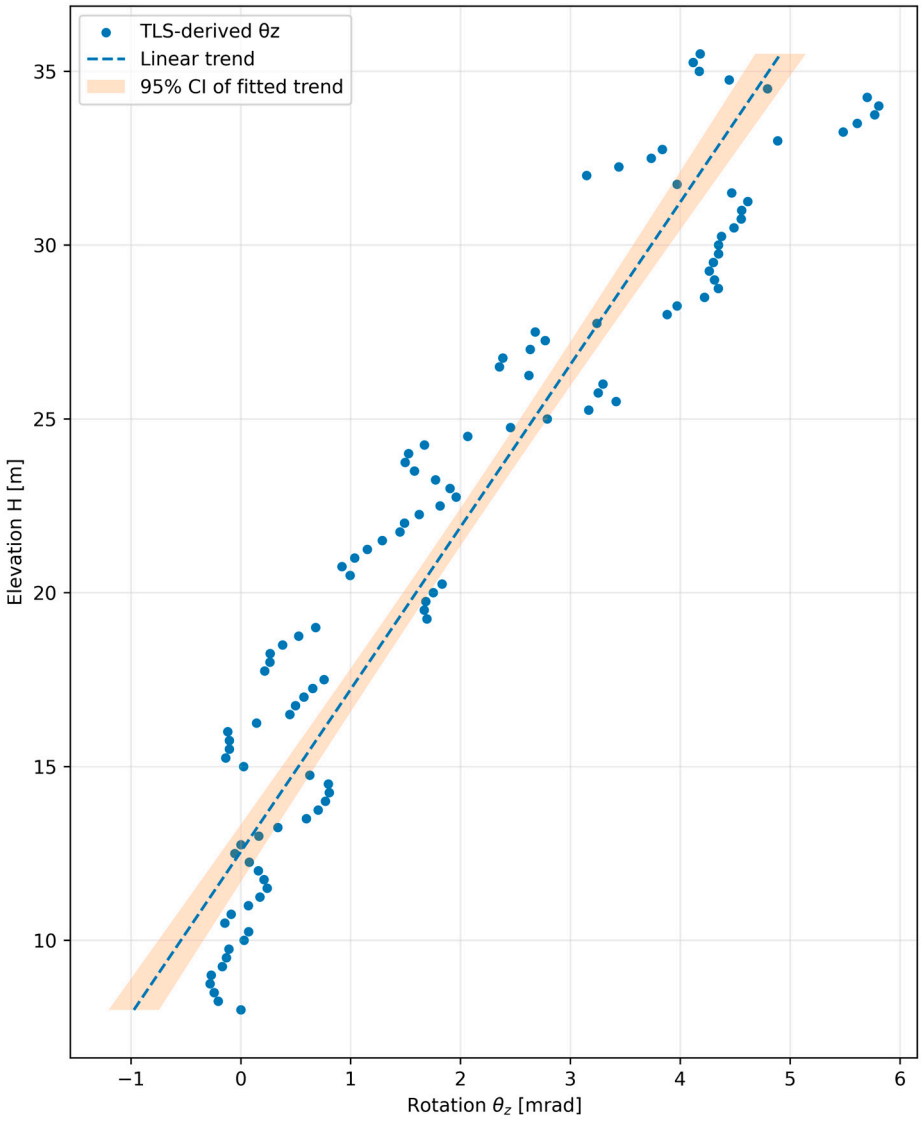


Figure 9. The variation in θz as a function of elevation. Points represent the rotational angles obtained from the TLS-based geometric analysis. The dashed line represents the fitted linear trend, and the shaded band denotes its 95% confidence interval.

The obtained profile shows an overall increasing trend in rotational angle with height, although local reversals are present at individual elevation levels. Based on 111 available cross-sectional estimates, linear regression yielded a positive slope of 0.214 mrad/m (95% CI: 0.200–0.228 mrad/m, $R^2 = 0.888$, $p < 0.001$). The positive monotonic relationship was additionally confirmed by Spearman's rank correlation ($\rho = 0.951$, $p < 0.001$), indicating that the observed local reversals do not alter the overall elevation-dependent increase in the rotational component. The rotation angle increases from approximately 0 mrad at the reference level to values exceeding 5 mrad in the upper part of the building. This height-dependent variation, together with the spatially variable displacement pattern, indicates a torsional component of the geometric deformation rather than merely differential linear displacement of individual corners. The statistical results are summarized in Table 4.

Table 4. Statistical assessment of the elevation-dependent θz trend based on 111 cross-sectional estimates.

Statistic	Value
Number of cross-sectional estimates, *n*	111
Linear regression slope [mrad/m]	0.214
95% CI of slope [mrad/m]	0.200–0.228
R^2	0.888
Regression *p*-value	<0.001
Spearman's ρ	0.951
Spearman's *p*-value	<0.001

The results indicate that the building experiences a global torsional component affecting the overall structural geometry. This phenomenon may be associated with differential foundation displacements induced by spatially variable ground deformation.

The identified rotational behaviour is consistent with the previously observed displacement patterns and further supports the interpretation of a complex structural response to non-uniform mining-induced ground movements.

5.5. Synthesis of Results

The conducted analysis demonstrates that the dominant displacement component occurs along the local Y-axis, which is consistent with the prevailing direction of ground inclination within the study area.

The deformation profile is distinctly non-linear and varies with elevation. Significant asymmetry of corner displacements was identified, together with an overall increasing torsional rotation with height, accompanied by local variations.

The highest displacement magnitudes were recorded at Corners 4, 6, and 7, confirming a non-uniform distribution of deformation across the building footprint.

The investigated structure does not behave as a rigid body subjected solely to uniform tilting. Instead, it exhibits a complex spatial response resulting from long-term interaction between mining-induced ground deformation and the structural behaviour of the building.

Furthermore, comparison with the theoretical ground deformation field indicates that the building response cannot be interpreted as a direct transfer of ground movements. Although the overall deformation direction remains consistent with the mining-induced deformation pattern, the magnitude and distribution of observed displacements are significantly modified by structural stiffness and by processes occurring within the soil–foundation–structure system [45].

6. Discussion

The obtained results clearly indicate that the current geometric condition of the analysed building is the result of long-term interaction between mining-induced ground deformation and the actual three-dimensional structural response of the building. The observed displacements cannot be interpreted solely as a simple global tilt, but also include differential deformation and a pronounced torsional component.

6.1. Assessment in the Context of Serviceability Limit States

The maximum local tilt ratio reached approximately 5.9 mm/m, which significantly exceeds values commonly regarded as acceptable for multi-storey residential buildings in engineering assessment practice. Tilt magnitudes of this order may result in reduced

serviceability, damage to non-structural components, malfunction of building installations, and increased stress concentrations within structural elements [16,17].

Consequently, the analysed structure may be considered to have exceeded typical serviceability criteria and should remain subject to further technical monitoring. In engineering practice, buildings exhibiting comparable levels of inclination may require remedial measures, including structural rectification procedures aimed at restoring verticality [46].

6.2. Deformation Mechanism: Tilting Versus Torsion

One of the most significant findings of this study is the considerable variation in corner displacements, ranging from 8.6 mm to 178.3 mm at the highest common measurement level. Such a displacement pattern is inconsistent with the behaviour of an ideal rigid body and indicates the simultaneous occurrence of several deformation mechanisms:

- Global building tilt;
- Differential foundation displacements;
- Rotation of the structure about the vertical axis;
- Local variations in structural stiffness.

In the adopted geometric interpretation, global tilting (rocking) is represented by the overall change in the position and inclination of the building relative to the reference level, whereas torsional deformation is represented by differential rotation of successive horizontal cross-sections about the vertical axis after removal of their translational component. Therefore, the presence of a large absolute displacement does not by itself indicate torsional deformation; torsion is identified from the residual rotational component θz and the spatial differences between cross-sections.

The statistically significant overall increase in the rotation angle θz with height, despite local variations in the profile, supports the interpretation of an elevation-dependent torsional component of the geometric deformation. This phenomenon is of practical importance because torsional deformations are generally more difficult to compensate than unidirectional tilting and may increase demands on structural connections and joints.

The identified torsional behaviour refers to the geometric rotation of successive cross-sections derived from TLS observations and should not be interpreted directly as a structural torsion state in the mechanical sense. The presented analysis describes the geometric response of the building rather than the distribution of internal stresses or torsional moments within the structural system.

6.3. Relationship Between Building Response and Mining-Induced Ground Deformation

Comparison of TLS-derived building displacements with the analysed ground deformation indicators (Figures 3–5) reveals a clear correspondence between the direction of building inclination, the distribution of ground tilt isolines (T), and the gradients of horizontal ground strain (ε).

Figure 10 compares the building axis derived from TLS measurements with the theoretical deformation profile predicted from the mining subsidence model. The comparison includes the last available modeled state (2014) and the historical maximum tilt values.

In the local X-direction, relatively good agreement was observed between the measured building geometry and the theoretical deformation model. This suggests that the structural response in this direction remains largely controlled by the kinematic forcing imposed by ground deformation.

A different behaviour was observed along the local Y-axis. The measured building inclination in this direction is generally smaller than the values predicted by both the last available modeled state (2014) and historical deformation models. This indicates that the structure does not fully replicate the deformation of the underlying ground. Instead, its

response is partially moderated by the spatial stiffness of the building, redistribution of internal stresses, and long-term adaptation processes occurring within the structural system.

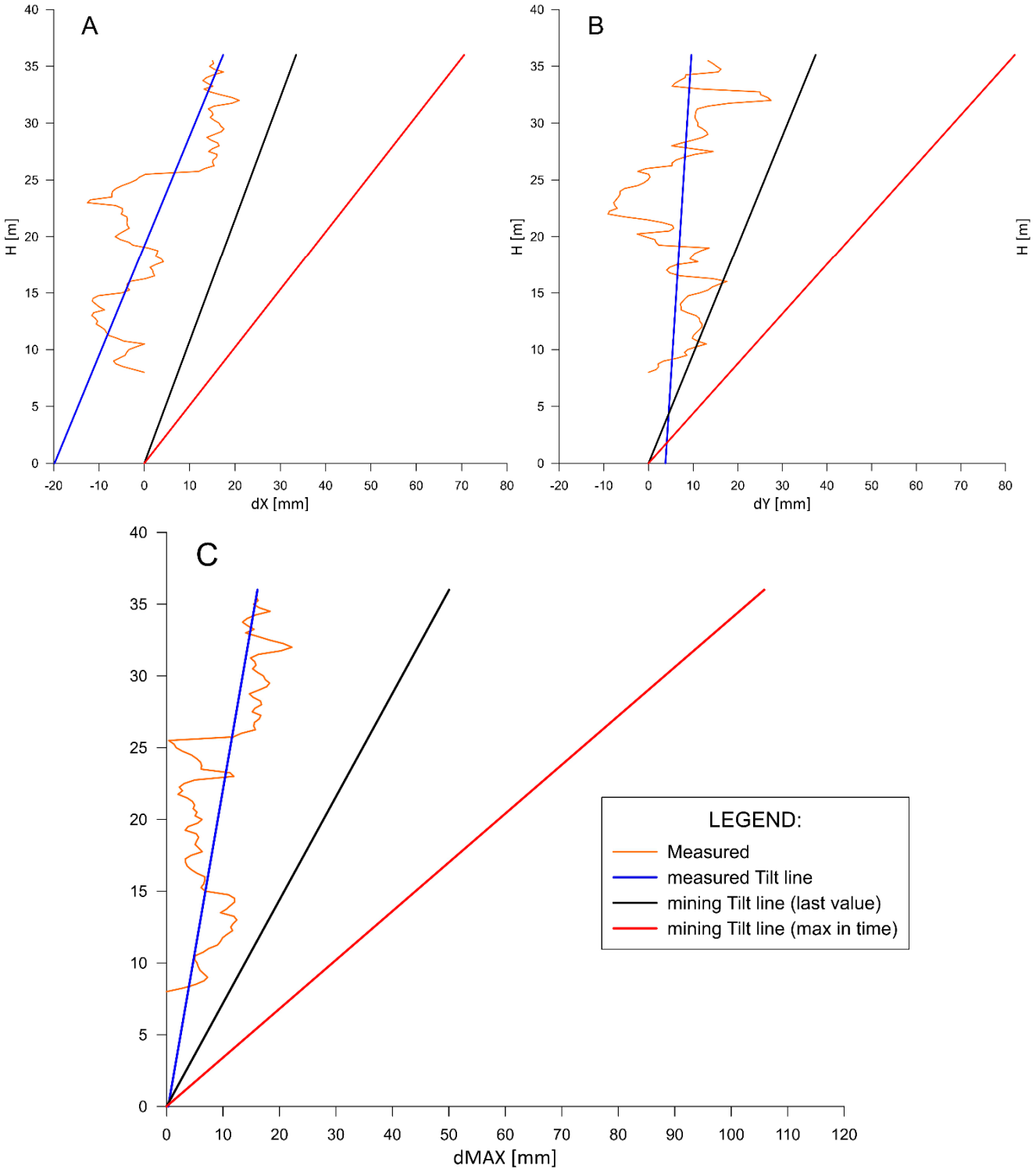


Figure 10. Comparison of the building axis derived from TLS data with the theoretical inclination profile predicted from the mining-induced ground deformation model: (**A**) displacements along the local X-axis, (**B**) displacements along the local Y-axis, and (**C**) maximum displacement values.

The largest discrepancies occur for the maximum displacement scenario shown in Figure 10C, where the historical theoretical tilt values considerably exceed the currently observed geometry of the building. This suggests that the present geometric condition

reflects not only the cumulative effects of mining-induced ground movements but also secondary structural processes such as stiffness redistribution, material creep, and gradual relaxation of structural connections.

These findings demonstrate that direct transfer of ground deformation indicators into predicted building deformation may lead to overestimation of the actual structural response. Similar relationships between ground movements and structural behaviour have previously been reported in both the Legnica–Głogów Copper District and the Upper Silesian Coal Basin [9,47].

However, the historical deformation model represents the period up to 2014, whereas the TLS survey represents the structural geometry observed in 2025. Therefore, the comparison should be interpreted as a comparison between the present structural geometry and the long-term geomechanical context rather than as a direct temporal validation of the model.

Detailed archival information linking individual historical mining panels or excavation fronts to specific damage events in the investigated building was not available. Therefore, the present study does not attempt to establish a one-to-one relationship between individual mining operations and individual structural defects. Instead, the analysis considers the cumulative ground-deformation field as the geomechanical forcing acting on the building over the long term. The contribution of individual historical mining-induced seismic events to the present deformation could not be quantified because sufficiently time-resolved structural observations were not available.

6.4. Interpretation of Structural Response to Ground Movements

Comparison of TLS-derived measurements with the theoretical ground deformation model indicates that the response of the analysed building is complex and cannot be interpreted as a simple linear transfer of ground deformation.

The displacement profiles exhibit a clear directional dependency. Along the X-axis, the structural response remains relatively consistent with the mining deformation model, whereas along the Y-axis the measured displacements are substantially smaller than the theoretical predictions. This behaviour indicates that the building partially compensates for ground-induced kinematic loading through its spatial stiffness and structural configuration.

Another important observation concerns the discrepancy between the current building geometry and the historical maximum ground tilt values. Although the deformation model suggests that larger ground inclinations may have occurred in the past, the present geometry does not directly reflect those extreme values. This may indicate the contribution of secondary processes such as stiffness redistribution, relaxation of prefabricated panel connections, and long-term rheological effects within reinforced concrete components.

The results further demonstrate that the structural response is not linearly proportional to the imposed ground deformation. Variations in displacement gradients with height, together with the identified torsional behaviour, indicate a highly complex three-dimensional response of the structural system.

The presented analysis highlights a fundamental limitation of traditional mining impact assessments based solely on ground deformation indicators. While such indicators describe the kinematic behaviour of the ground surface, they do not provide direct information regarding the actual response of a structure. TLS enables direct measurement of building geometry and facilitates the identification of deformation mechanisms that remain undetectable when relying exclusively on ground deformation models. The importance of considering the coupled interaction between ground movements and structural stiffness has also been emphasized in recent studies on soil–structure interaction [48].

One of the principal findings of this study is that the actual geometric response of the building does not represent a direct transfer of mining-induced ground deformation. Although the direction of inclination is generally consistent with the orientation of the ground deformation field, both the magnitude and spatial distribution of structural displacements are significantly modified by structural stiffness and by interactions within the soil–foundation–structure system.

These findings suggest that the assessment of high-rise buildings located in mining-affected areas should not rely exclusively on ground deformation indicators, but should also incorporate direct geometric measurements of the structure itself.

6.5. Significance of the Applied Methodology

The results confirm the effectiveness of the integrated TLS–total station approach for deformation assessment of buildings affected by mining activity. Terrestrial laser scanning provides a quasi-continuous representation of building geometry and enables identification of non-linear deformation phenomena that are often difficult or impossible to detect using conventional point-based surveying methods [18,26,28,49].

Unlike InSAR techniques, which primarily provide information on ground surface deformation, TLS allows direct assessment of the actual geometric response of an individual structure.

6.6. Limitations and Future Research

This study is based on a single measurement campaign, which limits the possibility of analysing temporal deformation evolution. In addition, the absence of detailed information regarding material properties and the condition of structural connections restricts the ability to separate mining-induced effects from ageing-related structural processes. Detailed information on soil stratification and geotechnical parameters directly beneath the investigated building was also not available and was therefore not included in the quantitative analysis. Furthermore, detailed archival information regarding subsequent renovations, repairs, and the complete history of structural damage was not available. These limitations should be considered when interpreting the observed geometric response.

Future investigations should therefore focus on:

- Implementation of periodic TLS monitoring campaigns;
- Integration of geodetic observations with finite element (FEM) models;
- Incorporation of inclinometer measurements;
- Deployment of continuous structural health monitoring sensors.

Future work should additionally focus on multi-epoch TLS monitoring integrated with geotechnical observations and numerical soil–structure interaction models, which would allow the temporal evolution of global tilt and torsional deformation to be assessed more directly.

Although the influence of construction tolerances and long-term material processes cannot be entirely excluded, the magnitude of the observed displacements and their directional agreement with the mining deformation field indicate that mining-induced ground deformation is an important contributor to the observed geometric response.

7. Conclusions

The conducted TLS-based spatial analysis of an eleven-storey large-panel residential building subjected to long-term mining influences leads to the following conclusions:

- Complex deformation mechanism of the structure. The investigated building does not behave as an ideally rigid body subjected solely to uniform tilt. In addition to a pronounced global inclination, differential corner displacements and an overall in-

crease in torsional rotation with height, accompanied by local variations in the rotation profile, were identified, indicating a complex three-dimensional structural response.

- The actual structural response differs from the theoretical ground deformation pattern. Comparison of TLS-derived displacements with the mining subsidence model demonstrated that the building does not directly reproduce the ground deformation field. The observed response is significantly modified by structural stiffness and soil–foundation–structure interaction, highlighting the limitations of assessments based solely on theoretical ground deformation indicators.
- Limitations of conventional indicator-based assessment. Evaluation of high-rise buildings in mining areas based exclusively on theoretical subsidence parameters may lead to overestimation or misinterpretation of actual structural behaviour, as it neglects the interaction mechanisms occurring within the soil–foundation–structure system.
- Advantages of three-dimensional geometric diagnostics. The integration of terrestrial laser scanning with a precise geodetic control network provides an effective tool for comprehensive geometric assessment of buildings affected by mining activity. The proposed methodology enables the identification of non-linear deformation mechanisms, including torsional behaviour and local geometric irregularities, which are difficult to detect using conventional point-based surveying techniques.

Future research should combine multi-epoch TLS observations with geotechnical monitoring and numerical soil–structure interaction modelling to further distinguish the temporal evolution of global tilt and torsional deformation.

The presented results demonstrate that TLS-based geometric analysis constitutes an effective tool for assessing the response of multi-storey buildings subjected to long-term mining-induced ground deformation.

Author Contributions: Conceptualization, R.G., A.K. and Z.M.; methodology, R.G.; software, R.G. and Z.M.; validation, R.G., A.K. and Z.M.; formal analysis, R.G.; investigation, R.G. and Z.M.; resources, R.G., A.K. and Z.M.; data curation, R.G. and Z.M.; writing—original draft preparation, R.G.; writing—review and editing, R.G., A.K. and Z.M.; visualization, R.G., A.K. and Z.M.; supervision, A.K. and Z.M.; project administration, R.G., A.K. and Z.M.; funding acquisition, none. All authors have read and agreed to the published version of the manuscript.

Funding: This research received no external funding.

Data Availability Statement: The data supporting the findings of this study are available from the authors upon reasonable request. The datasets include large-volume TLS point clouds, tachymetric measurements, and processed derivatives generated within the project. Due to their size and technical storage constraints, they are not publicly available. However, the data presented in the article are sufficient to support the reported analyses and conclusions.

Acknowledgments: During the preparation of this manuscript, the author used OpenAI ChatGPT 5.5 and Google Gemini 3.1 Pro exclusively for language refinement, clarity improvement, and editorial assistance. These tools were not used to generate scientific content, data analyses, interpretations, or conclusions. All outputs were reviewed and edited by the author, who takes full responsibility for the final content of the manuscript.

Conflicts of Interest: The authors declare no conflicts of interest.

References

1. Knothe, S. A profile equation for a definitely shaped subsidence trough (Równanie profilu ostatecznie wykształconej niecki osiadania). *Arch. Gór. Hut.* **1953**, *1*, 22–38. (In Polish)
2. Budryk, W. Determining the Magnitude of Horizontal Ground Deformations (Wyznaczanie wielkości poziomych odkształceń terenu). *Arch. Gór. Hut.* **1953**, *1*, 63–74. (In Polish)
3. Popiołek, E. *Protection of Mining Areas*; Wydawnictwa AGH: Kraków, Poland, 2009.

4. Kwiatek, J. *Ochrona Obiektów Budowlanych na Terenach Górniczych*; GIG: Katowice, Poland, 1997. (In Polish)
5. Strzałkowski, P.; Szafulera, K. Occurrence of linear discontinuous deformations in Upper Silesia (Poland) in conditions of intensive mining extraction—Case study. *Energies* **2020**, *13*, 1897. [CrossRef]
6. Ścigała, R.; Szafulera, K. Linear discontinuous deformations created on the surface as an effect of underground mining and local geological conditions—Case study. *Bull. Eng. Geol. Environ.* **2020**, *79*, 2059–2068. [CrossRef]
7. Yang, Z.; Li, Z.; Zhu, J.; Wang, Y.; Wu, L. Use of SAR/InSAR in Mining Deformation Monitoring, Parameter Inversion, and Forward Predictions: A Review. *IEEE Geosci. Remote Sens. Mag.* **2020**, *8*, 71–90. [CrossRef]
8. Hejmanowski, R.; Malinowska, A. Evaluation of reliability of subsidence prediction based on spatial statistical analysis. *Int. J. Rock Mech. Min. Sci.* **2009**, *46*, 432–438. [CrossRef]
9. Hejmanowski, R.; Malinowska, A.; Kwinta, A.; Patykowski, G. Prediction of land subsidence and deformations at copper ore underground mining site: Experiences and verification based on KGHM mines in Poland. In Proceedings of the 16th International Congress for Mine Surveying, Brisbane, Australia, 12–16 September 2016.
10. Antonielli, B.; Sciortino, A.; Scancella, S.; Bozzano, F.; Mazzanti, P. Tracking Deformation Processes at the Legnica Glogow Copper District (Poland) by Satellite InSAR—I: Room and Pillar Mine District. *Land* **2021**, *10*, 653. [CrossRef]
11. Cieślik, K.; Milczarek, W. Application of machine learning in forecasting the impact of mining deformation: A case study of underground copper mines in Poland. *Remote Sens.* **2022**, *14*, 4755. [CrossRef]
12. Perżyło, D. A new model for forecasting of land surface subsidence caused by underground extraction of deposits. *Int. J. Environ. Sci. Technol.* **2023**, *20*, 3733–3748. [CrossRef]
13. Paszek, J. Analysis of the model used to predict continuous deformations of the land surface in areas subject to discontinuous deformations—A case study. *Appl. Sci.* **2024**, *14*, 7676. [CrossRef]
14. Blachowski, J.; Wajs, J.; Walerysak, N.; Becker, M. Monitoring of Post-Mining Subsidence Using Airborne and Terrestrial Laser Scanning Approach. *Arch. Min. Sci.* **2024**, *69*, 395–412. [CrossRef]
15. Hejmanowski, R.; Malinowska, A.; Stoch, T.; Warchała, M. Mapa dynamiczna miasta Polkowice–projekt nowoczesnych pomiarów deformacji. In *Zeszyty Naukowe Politechniki Śląskiej*; Wydawnictwo Politechniki Śląskiej: Gliwice, Poland, 2007. (In Polish)
16. Boscardin, M.D.; Cording, E.J. Building response to excavation-induced settlement. *J. Geotech. Eng.* **1989**, *115*, 1–21. [CrossRef]
17. Son, M.; Cording, E.J. Evaluation of building stiffness for building response analysis to excavation-induced ground movements. *J. Geotech. Geoenvironmental Eng.* **2007**, *133*, 995–1002. [CrossRef]
18. Mukupa, W.; Roberts, G.W.; Hancock, C.M.; Al-Manasir, K. A review of the use of terrestrial laser scanning application for change detection and deformation monitoring of structures. *Surv. Rev.* **2017**, *49*, 99–116. [CrossRef]
19. Dong, Z.; Liang, F.; Yang, B.; Xu, Y.; Zang, Y.; Li, J.; Wang, Y.; Dai, W.; Fan, H.; Hyyppä, J. Registration of large-scale terrestrial laser scanner point clouds: A review and benchmark. *ISPRS J. Photogramm. Remote Sens.* **2020**, *163*, 327–342. [CrossRef]
20. Aryan, A.; Bosche, F.; Tang, P. Planning for terrestrial laser scanning in construction: A review. *Autom. Constr.* **2021**, *125*, 103551. [CrossRef]
21. Truong-Hong, L.; Lindenbergh, R.; Nguyen, T.A. Structural assessment using terrestrial laser scanning point clouds. *Int. J. Build. Pathol. Adapt.* **2021**, *40*, 345–379. [CrossRef]
22. Muralikrishnan, B. Performance evaluation of terrestrial laser scanners—A review. *Meas. Sci. Technol.* **2021**, *32*, 072001. [CrossRef] [PubMed]
23. Mohammadi, M.; Rashidi, M.; Mousavi, V.; Yu, Y.; Samali, B. Application of TLS Method in Digitization of Bridge Infrastructures: A Path to BrIM Development. *Remote Sens.* **2022**, *14*, 1148. [CrossRef]
24. Shen, N.; Wang, B.; Ma, H.; Zhao, X.; Zhou, Y.; Zhang, Z.; Xu, J. A review of terrestrial laser scanning (TLS)-based technologies for deformation monitoring in engineering. *Measurement* **2023**, *223*, 113684. [CrossRef]
25. Kregar, K.; Ambrožič, T.; Kogoj, D.; Vezočnik, R.; Marjetič, A. Determining the inclination of tall chimneys using the TPS and TLS approach. *Measurement* **2015**, *75*, 354–363. [CrossRef]
26. Popović, J.; Pandžić, J.; Pejić, M.; Vranić, P.; Milovanović, B.; Martinenko, A. Quantifying tall structure tilting trend through TLS-based 3D parametric modelling. *Measurement* **2022**, *188*, 110533. [CrossRef]
27. Siwiec, J.; Lenda, G. Integration of terrestrial laser scanning and structure from motion for the assessment of industrial chimney geometry. *Measurement* **2022**, *199*, 111404. [CrossRef]
28. Pleterski, Ž.; Rak, G.; Kregar, K. Determination of Chimney Non-Verticality from TLS Data Using RANSAC Method. *Remote Sens.* **2024**, *16*, 4541. [CrossRef]
29. Zhou, M.; Qin, Y.; Xie, Q.; Song, Q.; Lin, S.; Qin, L.; Zhou, Z.; Wu, G.; Yan, P. Tilt monitoring of super high-rise industrial heritage chimneys based on LiDAR point clouds. *Buildings* **2025**, *15*, 3046. [CrossRef]
30. Ilieva, M.; Rudziński, Ł.; Pawłuszek-Filipiak, K.; Lizurek, G.; Kudłacik, I.; Tondaś, D.; Olszewska, D. Combined Study of a Significant Mine Collapse Based on Seismological and Geodetic Data—29 January 2019, Rudna Mine, Poland. *Remote Sens.* **2020**, *12*, 1570. [CrossRef]

31. Kudłacik, I.; Kapłon, J.; Lizurek, G.; Crespi, M.; Kurpiński, G. High-rate GPS positioning for tracing anthropogenic seismic activity: The 29 January 2019 mining tremor in Legnica- Głogów Copper District, Poland. *Measurement* **2021**, *168*, 108396. [CrossRef]
32. Hejmanowski, R. Modeling of time dependent subsidence for coal and ore deposits. *Int. J. Coal Sci. Technol.* **2015**, *2*, 287–292. [CrossRef]
33. Lv, L.G.; Lu, M.; Ding, A.; Gao, G.; Gao, R.; Du, K. Residual deformation in mining subsidence area and its effect on buildings. *Front. Earth Sci.* **2023**, *11*, 1127862. [CrossRef]
34. Witkowski, W.T.; Łucka, M.; Guzy, A.; Sudhaus, H.; Barańska, A.; Hejmanowski, R. Impact of mining-induced seismicity on land subsidence occurrence. *Remote Sens. Environ.* **2024**, *301*, 113934. [CrossRef]
35. Misa, R.; Sroka, A.; Mrocheń, D. Evaluating Surface Stability for Sustainable Development Following Cessation of Mining Exploitation. *Sustainability* **2025**, *17*, 878. [CrossRef]
36. Głowacki, T.; Bortnowski, P. Long-term prediction of post-mining land deformation with XGBoost, Bayesian optimization, and time series feature engineering. *Measurement* **2025**, *259*, 119630. [CrossRef]
37. Hejmanowski, R. *Prognozowanie Deformacji Górotworu i Powierzchni Terenu na Bazie Uogólnionej Teorii Knothego dla Złóż Surowców Stałych, Ciekłych i Gazowych*; Instytut Gospodarki Surowcami Mineralnymi i Energią PAN: Kraków, Poland, 2001. (In Polish)
38. Malinowska, A.; Hejmanowski, R.; Dai, H. Ground movements modeling applying adjusted influence function. *Int. J. Min. Sci. Technol.* **2020**, *30*, 243–249. [CrossRef]
39. Misa, R. Knothe's theory parameters–computational models and examples of practical applications. *Mineral. Resour. Manag.* **2023**, *39*, 157–180. [CrossRef]
40. Ghilani, C.D. *Adjustment Computations: Spatial Data Analysis*; John Wiley & Sons: Hoboken, NJ, USA, 2017. [CrossRef]
41. Xu, Y.; Wang, Y.; Yang, J.; Zhang, J. Two-stage terrestrial laser scan planning framework for geometric measurement of civil infrastructures. *Measurement* **2025**, *242*, 115785. [CrossRef]
42. Xu, Y.; Stilla, U. Toward building and civil infrastructure reconstruction from point clouds: A review on data and key techniques. *IEEE J. Sel. Top. Appl. Earth Obs. Remote Sens.* **2021**, *14*, 2857–2885. [CrossRef]
43. Świerczyńska, E.J.; Wojda, D. Analysis of the impact of TLS point cloud feature sets on the detection of building displacements using machine learning algorithms. *Rep. Geod. Geoinform.* **2026**, *121*, 19–42. [CrossRef]
44. Besl, P.J.; McKay, N.D. A method for registration of 3-D shapes. *IEEE Trans. Pattern Anal. Mach. Intell.* **1992**, *14*, 239–256. [CrossRef]
45. Zonara, L.K.G.; Katsimpini, P.S. Nonlinear seismic response of a long-span suspension bridge under sequential ground motions considering pile foundation soil–structure interaction. *CivilEng* **2026**, *7*, 37. [CrossRef]
46. Gromysz, K. Rectification an 11-Storey Vertically Deflected Residential Building. *Procedia Eng.* **2013**, *57*, 382–391. [CrossRef]
47. Przyłucka, M.; Kowalski, Z.; Perski, Z. Twenty years of coal mining-induced subsidence in the Upper Silesia in Poland identified using InSAR. *Int. J. Coal Sci. Technol.* **2022**, *9*, 86. [CrossRef]
48. Zhang, C.; Wu, K.; Huang, S.; Li, L.; Rao, X. Study on the simulation of bridge deformation in a mining subsidence area. *Sci. Rep.* **2025**, *15*, 529. [CrossRef] [PubMed]
49. Lenda, G.; Marmol, U. Integration of high-precision UAV laser scanning and terrestrial scanning measurements for determining the shape of a water tower. *Measurement* **2023**, *218*, 113178. [CrossRef]

Disclaimer/Publisher's Note: The statements, opinions and data contained in all publications are solely those of the individual author(s) and contributor(s) and not of MDPI and/or the editor(s). MDPI and/or the editor(s) disclaim responsibility for any injury to people or property resulting from any ideas, methods, instructions or products referred to in the content.